In-situ phosphatization and enhanced corrosion properties of films made of phosphate functionalized nanoparticles

Stefano Chimenti [1], *Jesús Manuel Vega* [2], *Eva García-Lecina* [2], *Hans-Jürgen Grande* [2,3], *María Paulis* *[1], *Jose Ramón Leiza* *[1].

1: POLYMAT, Kimika Aplikatua saila, Kimika Fakultatea, University of the Basque Country UPV/EHU, Joxe Mari Korta Zentroa, Tolosa Hiribidea 72, 20018 Donostia-San Sebastián, Spain.

2: CIDETEC, Parque Científico y Tecnológico de Gipuzkoa, Po. Miramón 196, 20014 Donostia-San Sebastian, Spain

3: POLYMAT, Polymer Science and Technology Department, Faculty of Chemistry, University of the Basque Country (UPV/EHU), 20018 Donostia-San Sebastian, Spain

*maria.paulis@ehu.eus, jrleiza@ehu.eus

ABSTRACT

In the present work a thin, stand-alone waterborne coating with excellent anticorrosion performance was successfully designed thanks to a built-in ability to in-situ phosphatize low carbon steel substrates. During film formation, the phosphate functionalities, incorporated by using a phosphate functional surfmer, were able to interact with steel leading to a thin iron phosphate passive layer at the coating-metal interface, as proven by SEM-EDX, FTIR and XPS. The phosphatization layer that plays a key role on the excellent anticorrosion properties obtained (measured by EIS analysis of coated sample immersed in 3.5 wt% NaCl solution and in an aggressive salt spray chamber), strongly depends on the humidity at which the waterborne dispersion is applied; at relative humidity above 60%, optimum performance is achieved.

KEYWORDS Waterborne binder, phosphate surfmer, anticorrosion, film formation, in-situ phosphatization

ABBREVIATIONS

MMA, Methyl methacrylate; BA, n-Butyl acrylate; KPS potassium persulfate; DOW, Dowfax 2A1; SIP, Sipomer PAM200; DLS dynamic light scattering; EIS, electrochemical impedance spectroscopy; SEM, scanning electrical microscopy; EDX energy dispersive X-ray spectroscopy; FTIR; Fourier Transform Infrared spectroscopy; RH, relative humidity, XPS X-ray photoelectron spectroscopy.

1. INTRODUCTION

Mild steel is used as primary constructional material in many sectors such as transportation, infrastructures and utilities. However, it is very much prone to corrosion and its protection against deterioration is challenging and necessary. Wet corrosion can be defined as an electrochemical process that degrades the surface of a metal by dissolution reactions combined with the formation of corrosion products [1, 2]. Moreover, it is a very fast process that causes lots of economic losses; according to NACE International, the global cost of corrosion was estimated to be US$2.5 trillion, which is equivalent to 3.4% of the global GDP (2013)[3]. Therefore, the prevention of corrosion is still one of the main challenges of the XXIst century and one of the strategies where the scientific community is devoting large effort is the development of protective organic coatings [4-8]. Industrial organic coatings tailored for corrosion protection must offer a physical barrier, impeding the diffusion of corrosive species to the metal surface, and the inhibition of the corrosion reactions that threaten the underlying metal.

Generally, coating systems are solvent based but, due to environmental regulation requirements and sustainability [9-11], waterborne coatings have become increasingly interesting in the coating industries thanks to their low content in volatile organic compounds (VOC). Among the waterborne coatings, acrylic latexes play an important role due to their good film formation and weatherability [12-14]. Since waterborne coatings present worse water resistant properties compared to their solvent based counterparts, solvent-borne coatings remain the preferred choice in corrosion protection because they continue to offer exceptional barrier performances in a wide range of environmental conditions. In fact, in films cast from waterborne latexes, the presence of surfactants or salts, that are not totally exuded during the film formation, cause higher diffusion of water

through the film and impair the ability to prevent the corrosion [15-20]. Nevertheless, as shown in literature, the reduction of water sensitivity can be partially overcome by incorporating polymerizable surfactants in the latex formulation [17, 18, 21]. Another drawback of waterborne coatings for corrosion protection, that is worth considering, is the flash rust corrosion [22]. This phenomenon appears quickly, especially when thin water films reside on the metal surface triggering the corrosive action. Due to that, in order to prevent flash rust corrosion from taking place [7, 23], unlike solventborne system, conversion coating layers are always considered in the design of the protective coatings based on waterborne binders.

Some attempts to design a waterborne primer with a conversion coating built-in have been done to reduce the number of layers. Lin et al. reported an in situ phosphatizing system in which a phosphatizing agent is pre-mixed with the coating [24-27]. However, it is worth to mention that if the phosphating agent is not homogenously dispersed, the corrosion protection can be affected and a possible agglomeration of the phosphating agent can also cause the formation of defects in the resulting protective film. Del Donno [28] discussed the enhanced adhesion on metal substrate of polymer containing phosphorus pendant chains. Based on that, in order to have homogeneous distribution of phosphate functionalities in the coating and to enhance the adhesion on the metal substrate, the incorporation of phosphate functionality into the resin in the form of surfactant [29] or monomer [30] was studied. Although better adhesion has been reported, none of these systems has demonstrated to be able to protect the metal substrate in formulations without anti-corrosion pigments. Some stand-alone single layered epoxy barrier coatings with thicknesses in the range of 250 µm have been studied and reported in literature [8, 31]; however, in these cases, anticorrosion inhibitor pigments were always mixed with the polymer and in some cases they triggered the degradation of the polymeric matrices [32].

In the present work, we attempt to develop a thin stand-alone single layer barrier coating by synthesizing a versatile waterborne binder (which fulfills the environmental standard established related to VOCs levels), with multifunctional capabilities such as metal/coating interface adhesion/passivation and barrier protection, typical of a conversion coating and primer-topcoat respectively, and that is able to protect the metal substrate without the aid of any corrosion inhibitors. Waterborne polymeric dispersions, made of a copolymer of methyl methacrylate (MMA) and butyl acrylate (BA) containing phosphated functionalities has been synthetized using a phosphated surfmer. The optimal drying conditions that lead to in-situ phosphatization of the metal-coating interface have been investigated and the anticorrosion protection has been evaluated in both mild (NaCl 3.5 wt% solution) and harsh corrosive environments (salt-spray exposure to 5 wt% NaCl salty fog), respectively. The performance of these binders was compared with a binder synthetized using conventional anionic surfactant. For all the tested samples, electrochemical impedance spectroscopy (EIS) has been used as non-destructive test to monitor the evolution of the coating with time.

2. MATERIALS AND METHODS

2.1 Materials

Methyl methacrylate (MMA) and n-butyl acrylate (BA) (Quimidroga) were used as received. Dodecyl diphenyloxide disulfonate (Dowfax 2A1 45%, Dow Chemical company, DOW) was used as anionic emulsifier. Phosphate esters of polypropylene glycol monomethacrylate (Sipomer® PAM200, Solvay, SIP) was used as surfmer. Sipomer® PAM 200 is a surfmer characterized by a short polypropylene glycol chain (Mn = 500 g/mol) with a polymerizable acrylic end group and a phosphate group as polar chain end. Potassium persulfate (KPS, Fluka) radical initiator was used

as received. Deionized water (MiliQ quality) was used in all reactions. Steel substrates (low carbon steel with 0.5% of C) were purchased from Urduri S.L. UniClean 251 (Atotech) was used as degreasing agent for the steel substrates. HCl 1M solution (Aldrich) was used in the cleaning treatment of the steel substrates.

2.2 Synthesis of phosphated Poly (MMA-co-BA) waterborne dispersions

All the latexes were synthetized by seeded semibatch emulsion polymerization and the recipes are summarized in Tables 1 and 2. The synthesis of the seed (labeled MB) with a solids content of 13 %, was carried out in a 1L glass-jacketed reactor (equipped with reflux condenser, feeding and sampling outlet and stainless steel impeller rotating at 200 rpm) under a N_2 atmosphere at 70 °C, in semibatch conditions by feeding the monomer during 4 hours and allowing the latex to react for one more hour under batch conditions. The seeded semibatch emulsion polymerization was carried out in the same glass-jacketed reactor. In detail, the experimental procedure to achieve a latex of 50 % solids content was as follows; the seed was added into the reactor and heated up to the target reaction temperature of 70 °C. Once the temperature was reached, the initiator (KPS) was added and a monomer preemulsion (containing the monomers, water and Sipomer PAM200 (SIP) or Dowfax 2A1 (DOW)) was fed to the reactor for 4 hours. pH neutralization, by addition of ammonia solution, of the preemulsion containing SIP was necessary to incorporate the surfmer into the system as very acid or very basic conditions would hydrolyze the ester linkage of the phosphate group. Upon finishing the feeding, the reaction was post-polymerized for one hour to reduce the amount of unreacted monomers. The latex synthetized with SIP is labeled as MB_S and the one with DOW as MB_D (see Table 2).

Table 1. MB seed formulation

Reagent	*Initial load* (g)	*Stream* (g)
MMA	-	31.3
BA	-	31.3
Water	436.7	-
DOW	0.630	-
KPS	0.313	-
$NaHCO_3$	1.035	-

Table 2. Formulation used to synthetize MB_S and MB_D waterborne binders

LATEX	MB (seed)(g)	MMA(g)	BA(g)	KPS(g)	DOW(g)	SIP(g)	Water(g)	S.C.(%)
MB_S	107	119	119	0.313	/	5	149.77	50
MB_D	107	119	119	0.313	5	/	149.77	50

2.3 Characterization methods

Monomer conversion was determined by gravimetry. Polymer particle size distributions were measured by Dynamic Light Scattering (DLS) using a Zetasizer Nano Series (Malvern instrument). For this analysis, a fraction of latex was diluted with deionized water. The reported z-average particle size values represent an average of two repeated measurements. Regarding the latex films, different properties were investigated. The latexes were cast onto steel substrates and their anticorrosion properties were studied. Before casting the latex, steel substrates were degreased with UniClean 251 solution at 70 °C in a shaking bath for 5 minutes followed by 1 min decaping in HCl solution (1:1). Then the waterborne latexes were uniformly applied on the steel substrates

obtaining thicknesses around 40 µm. The films were applied with quadruple film applicator (Khushbooscientific).

Latex drying tests on the steel substrates were carried out using a temperature and humidity chamber (ESPEC SH-641), maintaining the temperature at 23 °C and controlling the drying rate by changing the relative humidity (RH: 30, 43, 50, 60 %).

SEM with X-Ray diffraction (SEM-EDX) was used to visualize the morphology of the coatings and to analyze the interface between the coating and the substrate in terms of its chemical composition. The coating was detached from the steel surface by immersion in liquid nitrogen after being applied under different drying conditions. All the measurements were performed using a bench top SEM 3030 Hitachi operating at 15 kV and at low vacuum. Furthermore, the composition profile of the coating applied onto the steel substrate and that of the substrate below was obtained using a Quantax EDS Bruker.

The FTIR absorption spectra of the coatings detached from the steel substrate were recorded using a Bruker Single reflection ATR with Platinum module in the range of wavelength comprised within 400 and 4000 cm^{-1}. The samples were prepared according to the same procedure described in the SEM_EDX analysis. The XPS spectra of the coatings detached from the steel substrates were recorded in a SPECS (Berlin, Germany) equipped with a Phoibos 150 1D-DLD detector and a monochromatic radiation Al Kα (1486.7 eV).

Electrochemical tests were performed using a multichannel potentiostat BIO-LOGIC VMP3 to evaluate the corrosion behaviour of the systems. A typical three electrodes cell, with a saturated Ag/AgCl (saturated with KCl) as reference electrode, platinum mesh counter electrode and the different coatings (cast from the synthetized latex) as working electrode were used. Electrochemical experiments were carried out at least by triplicate using an area of 1 cm^2. The

electrochemical tests were conducted in 3.5 wt% NaCl solution at room temperature. OCP (open circuit potential) was measured continuously with time although it was interrupted to carry out EIS measurements (once per hour). Frequency scans were carried out by applying ± 10 mV sinusoidal wave perturbation versus OCP. The frequency range was from 100 Hz to 10 mHz, obtaining 10 points per decade. Three specimens were used to perform neutral salt spray tests (NSS) for each system. Experiment were conducted using a DYCOMETAL MODEL SCC-400 salt spray chamber for 800 h. Test parameters were set according to ASTM B117 standard. Visual evaluation was carried out according to ISO 10289:1999 standard.

3. RESULTS AND DISCUSSION

3.1 Synthesis of phosphated poly(MMA-co-BA) waterborne dispersions

Stable poly(MMA-co-BA) seed latex with 13 % of solids content and average particle size of 65 nm was successfully synthetized by semibatch emulsion polymerization and then used for the synthesis of the final waterborne MB acrylic dispersions. Poly(MMA-co-BA) latexes with 50% of solids content and target particle size of around 190 nm (189 nm and 187 for MB_S and MB_D, respectively) were synthetized by seeded semibatch emulsion polymerization using conventional or polymerizable surfactants (latexes labeled MB_D and MB_S) (See Supporting Information for the morphological characterization of the final latex particles).

Despite the use of a surfmer can result in surfactant burial or formation of oligomers in the aqueous phase [21, 33] with consequent emulsion destabilization, SIP was successfully incorporated in the final latex obtaining particle sizes close to the target one. Moreover, this is an indirect proof that the number of polymer particles remained constant along the polymerization; namely, that neither secondary nucleation nor coagulation phenomena occurred during the reaction. In addition,

the use of polymerizable surfactant (SIP) had not remarkable effects neither on the polymerization kinetics nor on the mechanical properties of the resulting films (see Supporting Information).

3.2 Coating properties and in-situ phosphatization

3.2.1 Film formation on the metal substrate

In order to evaluate the anticorrosion performance, MB_D and MB_S latexes were applied, at 23 °C and 60% of relative humidity (RH), on steel substrates, previously cleaned, and the resulting coatings are shown in Figure 1. As it can be seen, when MB_D was cast, brown inhomogeneous stains (Figure 1a), typical of the flash rust, appeared on the steel surface. Indeed, sulfonate groups (belonging to the anionic surfactant Dowfax), in presence of water, can interact with the metal substrate forming iron complexes typically called green rust [34-36]. On the other hand, when MB_S binder was used (Figure 1b), a homogeneous yellowish stain appeared on the surface of the steel, presumably due to the interaction between the phosphate groups of the latex and the steel surface. The probable explanation behind this effect is the strong interfacial acid-base interactions of PO^{m-} groups with the Fe^{n+} [37]. In fact, at neutral pH conditions, orthophosphate ions ($RHPO_4^-$ and RPO_4^{2-}) may interact with the hydroxyl groups present on the metal surface forming a dense and thin iron phosphate passivating layer (Figure 2).

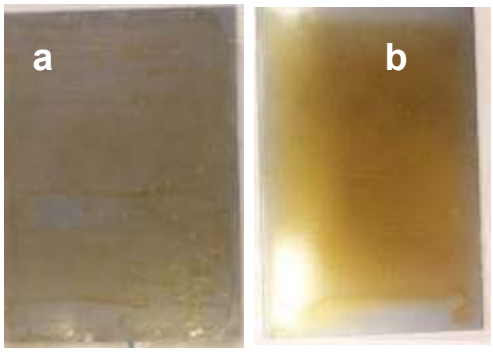

Figure 1. Steel substrates coated with MB_D (a) and MB_S (b) at 23 °C and RH= 60%.

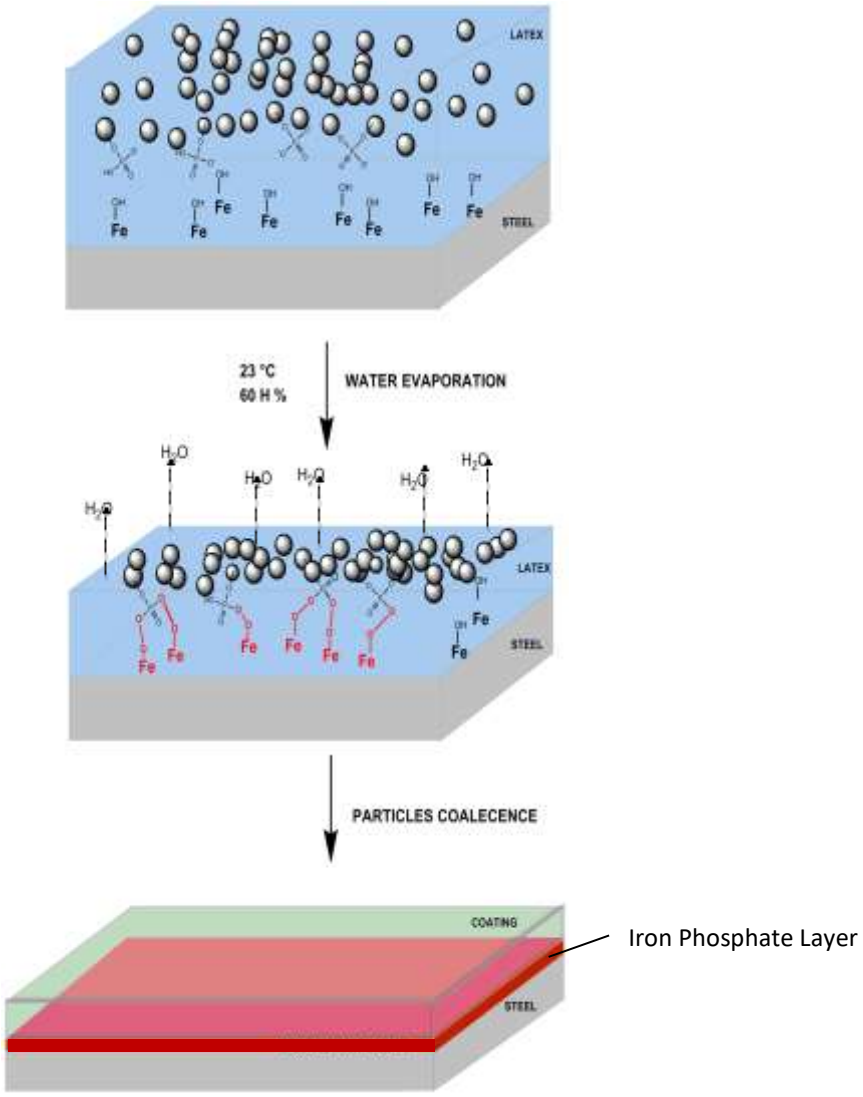

Figure 2. Schematic drawing of the in-situ phosphatization mechanism during latex film formation.

However, it has to be pointed out that this phenomenon was severely affected by the drying conditions. Figure 3 presents the different coatings obtained when the latex was cast on steel substrates at different drying conditions; namely, maintaining constant the drying temperature at 23ºC and changing the relative humidity (RH %) from 30% to 60%.

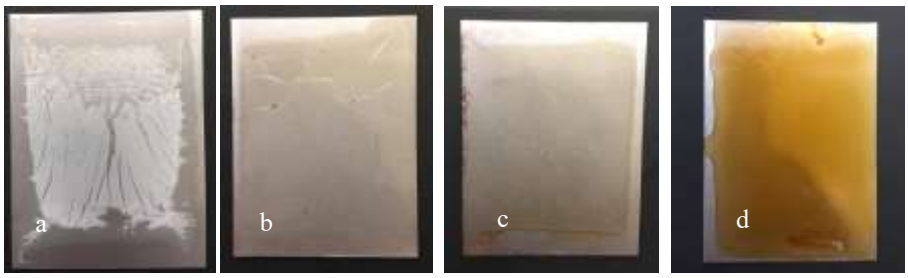

Figure 3. MB_S cast on steel substrates at different drying conditions; T=23 ºC (constant), a) RH=30%, b) RH=43%, c) RH=50%, d) RH=60%

According to the film formation mechanism [38-41], during the water evaporation, latex particles pack, deform and eventually coalescence (See Supporting Information for detailed information about the film formation process and the drying kinetics of the synthetized systems). Depending on the latex composition (e.g. monomers and surfactants), substrate, temperature of drying and the rate at which water evaporation occurs, different qualities of films can be obtained. In our study the drying temperature was maintained at a constant value of 23 °C, low enough to avoid the formation of superficial defects, related to a drastic evaporation of the water, and to avoid the skin layer formation due to the faster evaporation of water compared to particles diffusion. The drying rate was changed by means of variations of relative humidity (RH). As it can be seen in Figure 3, in-situ phosphatization with a good film formation was favored by decreasing drying rate (best layers obtained at 60% RH)). At higher drying rate (RH < 60%) the phosphatization did not have enough time to occur (Figure 3b and 3c). Moreover, if the RH was reduced to 30%, the film formation was affected as confirmed by the presence of fractures on the film surface. This observation might indicate that above 60% RH (i.e. good film formation) a deformation by wet or capillary sintering occurs, which is avoided when water evaporation is too fast (30% RH).

3.2.2 Coating-metal interface characterization by SEM-EDX

In order to investigate the coating-steel interface when drying at different rates, SEM-EDX analyses of the coating (at coating/steel interface) and of the steel surface below the coating were performed. After detaching MB_S dried at low rates (T= 23 °C and RH=60%, coating from Figure 3.d), the metal surface resulted rust-free, which was confirmed by SEM (Figure 4a), and by the elemental composition analysis (EDX) (Figure 4b). The oxygen peak centered at 0.53 KeV had lower intensity than the iron peak at 0.7 KeV and the composition extrapolated from the EDX pattern showed a Fe/O ratio of 92/8, which is consistent with the absence of rust. However, contrary to our expectations, the EDX spectra did not show any characteristic peak for phosphorous atoms and hence any signs of the presence of iron phosphate layer. Nevertheless, evidences of the interface phosphatization were found in the analysis of the detached polymeric film (MB_S). In fact, in the EDX spectra of the coating, in the side that had been in contact with the steel (Figure 5), the characteristic peaks of iron, centered at 0.7, 6.2 and 7.0 KeV, are clearly visible, together with the peak corresponding to phosphorous at 2.0 KeV. This suggests that the superficial iron is covalently bonded to the coating and when the coating is detached from the steel surface, the iron phosphates stay attached to the polymeric coating.

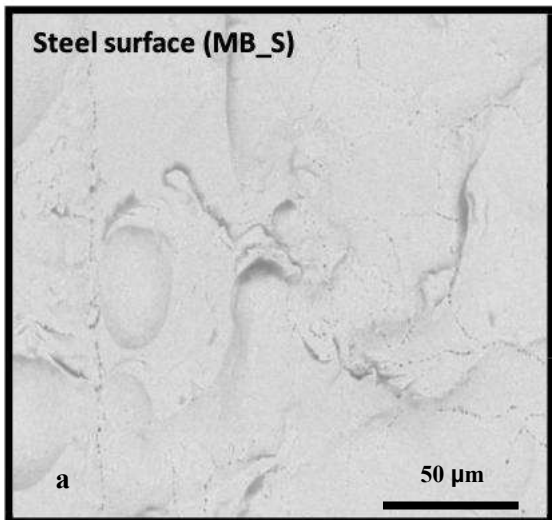

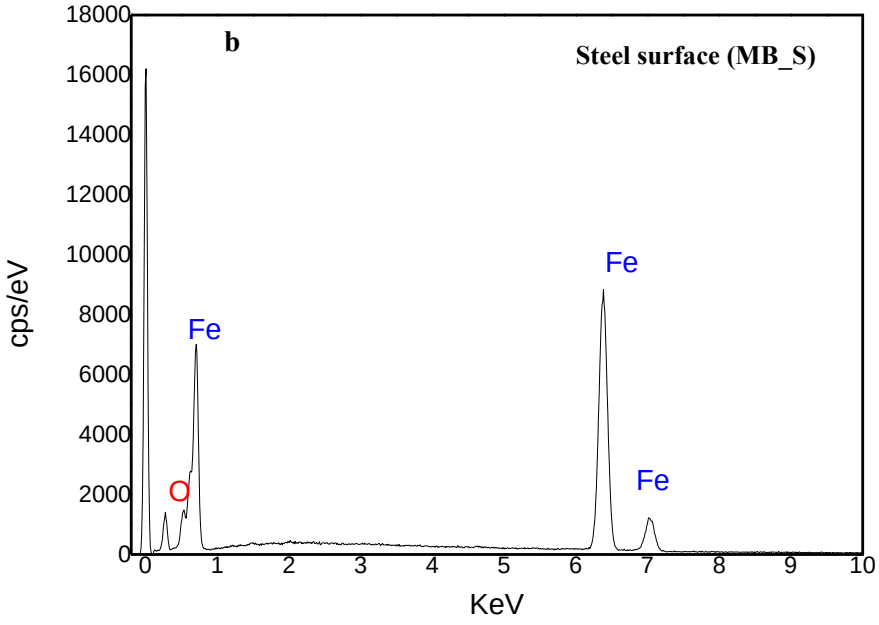

Figure 4. a) SEM micrograph and b) EDX pattern of steel surface after detaching MB_S coating (dried at 60 % RH).

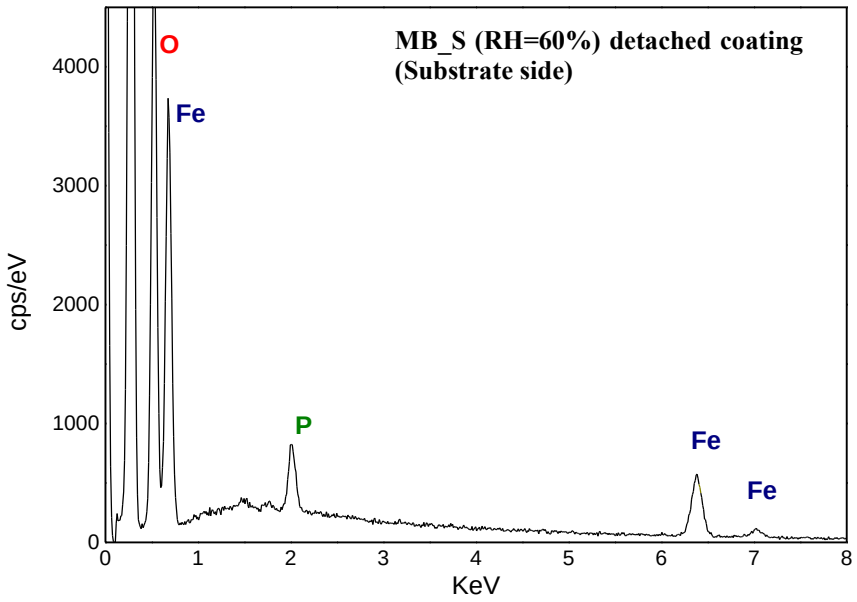

Figure 5. EDX spectra of MB_S coat detached from on steel substrate after casting the latex at low drying rate (RH=60%).

In the case of the latex cast at higher drying rate (RH = 43%, coating from Figure 3.b) (Figure 6), no peaks of iron were detected at the coating interface, confirming that drying conditions have a key role in the generation of the iron phosphate layer. According to these results, it was evident that lower drying rates allowed the formation of more homogeneous films and promote the strong interaction of the phosphate groups of the surfactant with the substrate.

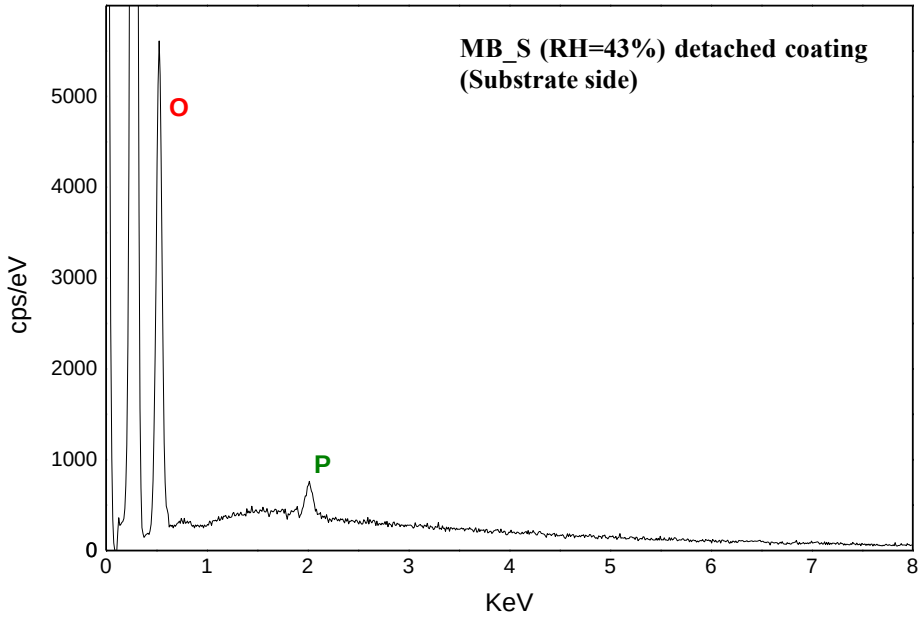

Figure 6. EDX pattern of MB_S coat detached from on steel substrate after casting the latex at high drying rate (RH=43%).

For comparison purposes, the same analysis was carried out for a steel substrate after detaching the film cast from MB_D latex. As it can be seen in Figure 7a, the SEM micrograph shows a grain-like agglomerate that resembles the morphology of Lepidocrocite (γ-FeOOH), which is one of the main components of flash rust [42, 43]. This finding is also confirmed in the EDX pattern, reported in Figure7b, by the higher intensity of the O peak (0.53 KeV) with respect to the one of Fe (0.7 KeV) which was consistent with the composition of corrosion products [42] .

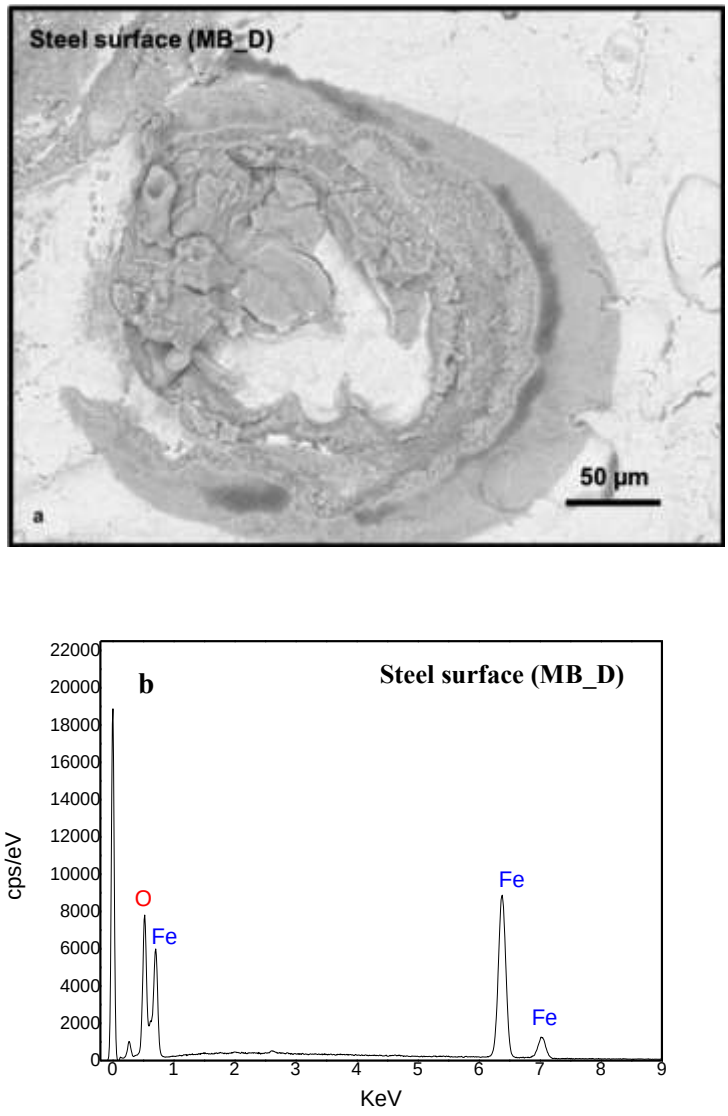

Figure 7. a) SEM micrograph and b) EDX pattern of steel surface after detaching MB_D coating (dried at 60 % RH).

3.2.3 Coating and coating-metal interface characterization by FTIR and XPS

Additional evidence of the in-situ phosphatization was provided by FTIR analysis of the coatings, cast from MB_S, within the range of 400-4000 cm^{-1}. Figure 8 shows the FTIR absorption spectra of the surface of the detached coating, cast from MB_S under low drying rate (RH=60%), at the coating-air (a) and coating-steel (b) interface respectively. The difference in composition

between the coating-air and the coating-steel interface was indicated in the spectrum b) by the stretching and bending vibrations bands of water molecules at 3300-3400 cm^{-1} and 1600 cm^{-1}, respectively [44-47]. These bands suggest the presence of chemisorbed water at the coating-steel substrate, which is consistent with the formation of hydrated iron phosphate layer; in fact, it is reported in literature, that the iron phosphate is generally produced in its hydrated forms such as Hureaulite ($Fe_3H_2(PO_4)_4$ $4H_2O$) or Strengite ($FePO_4$ $2H_2O$) [44]. In the low wavenumber region of both spectra a) and b) (from 1100 to 400 cm^{-1}), we identify internal modes of phosphates anions that belong to the phosphate group of SIP; namely the symmetric stretching vibration at 900 cm^{-1}, the asymmetric stretching in the regions of 990-1000 cm^{-1} (Figure 8) and the symmetric bending at 430-510 cm^{-1} (Figure 9) [44-48]. Furthermore, the presence of Fe in the coating-steel interface (spectrum b, Figure 9) is corroborated by the formation of new absorption bands in the region of 430-510 cm^{-1}; a shoulder at 430 cm^{-1} which was assigned to Fe-O bending vibration, and the peaks at 455 cm^{-1} and 495 cm^{-1} that were induced by the correlation effect of Fe-O units with phosphate anions [46, 48]. In addition, the peak at 620 cm^{-1} (spectrum b), that partially overlap the doublet at 620-630 cm^{-1} (assigned to C-O and C=O vibrations out of the plane [49]), was assigned to the stretching vibration of Fe-O [47]. Same analysis was carried out for MB_S coating dried at high drying rate (RH=43%). According to our expectation, the spectra of the film surface at the coating-air and coating-steel interface were very similar confirming the absence of the iron phosphate layer (see Supporting Information).

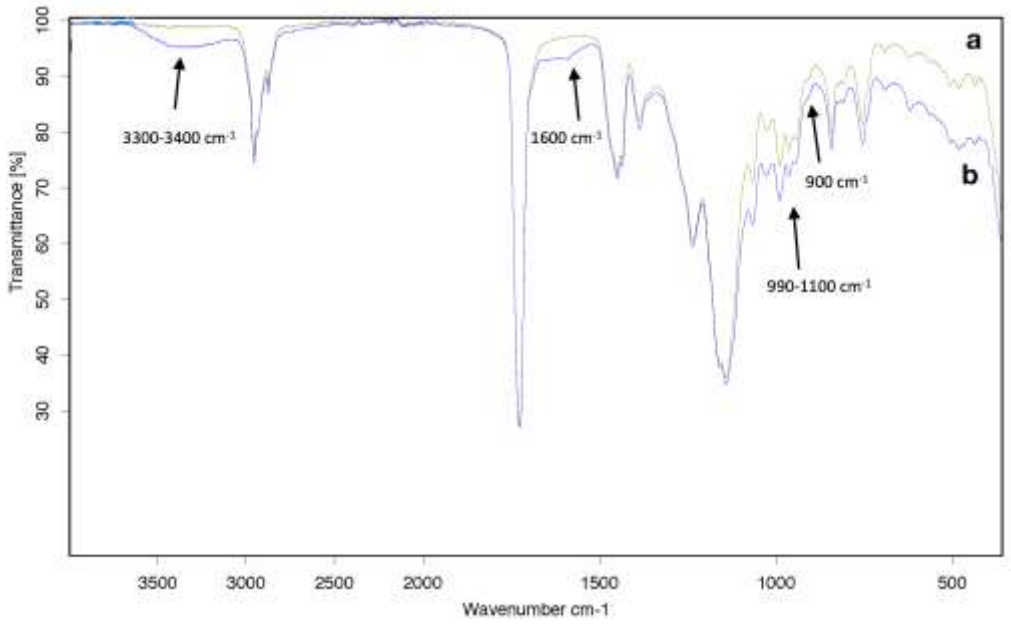

Figure 8. FTIR spectra of the MB_S (dried at RH=60%) surface at detached a) coating-air interface and b) coating-steel interface.

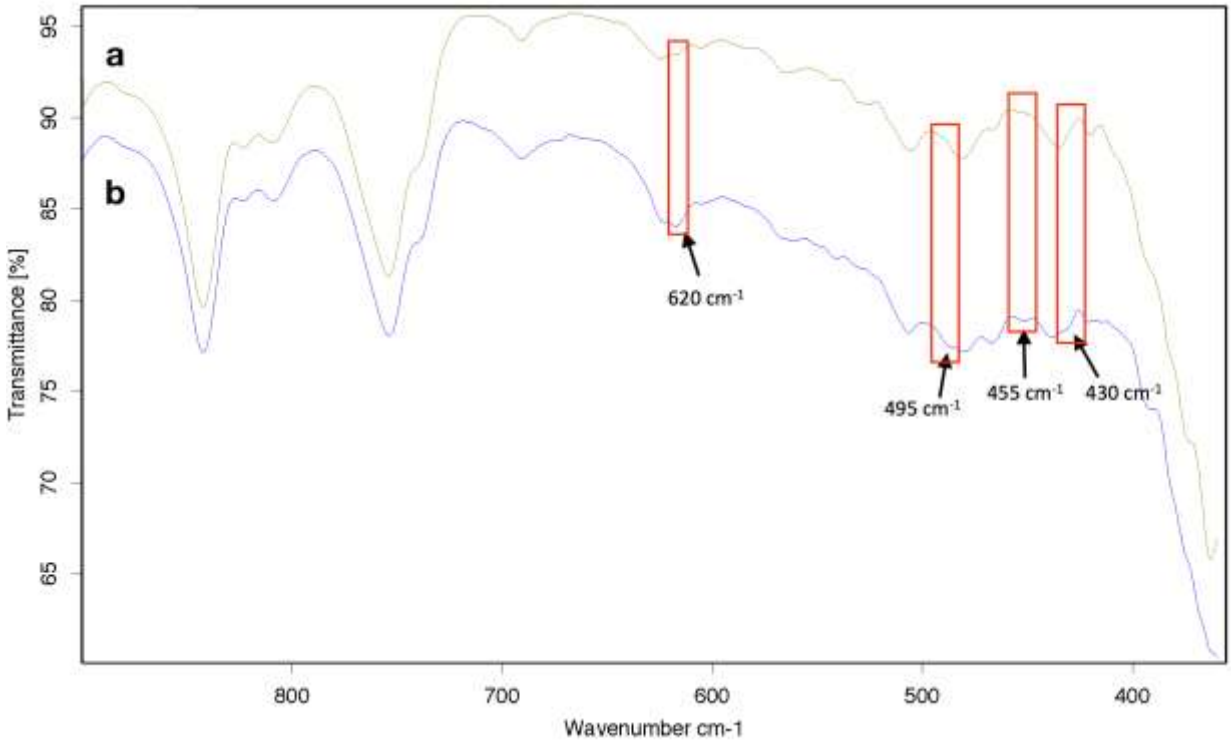

Figure 9. FTIR spectra at high wavenumber region of the MB_S (dried at RH=60%) surface at detached a) coating-air interface and b) coating-steel interface.

Further qualitative characterization of the phosphatization layer was provided by XPS analysis. Figure 10 shows the X-rays pattern, between 600 and 900 eV, of the detached MB_S and MB_D coatings respectively (see Supporting information for the entire XPS patterns for MB_S and MB_D detached coating). At first glance both patterns show the presence of characteristic iron (Fe2P) peaks; however, the low intensity of the peaks detected in the MB_S sample may indicate the formation of a thin iron phosphate layer whereas in MB_D sample, the higher intensity of the Fe peaks can be explained by the higher extent of iron oxidation characteristic of the flash rust. In addition to that, the Fe peaks in MB_S sample resulted centered at higher binding energy (711.8 – 731.8 eV) than those of MB_D sample (710.5 – 724.6 eV), which is consistent with the presence of iron phosphate instead of the iron oxide of the flash rust.[50-52].

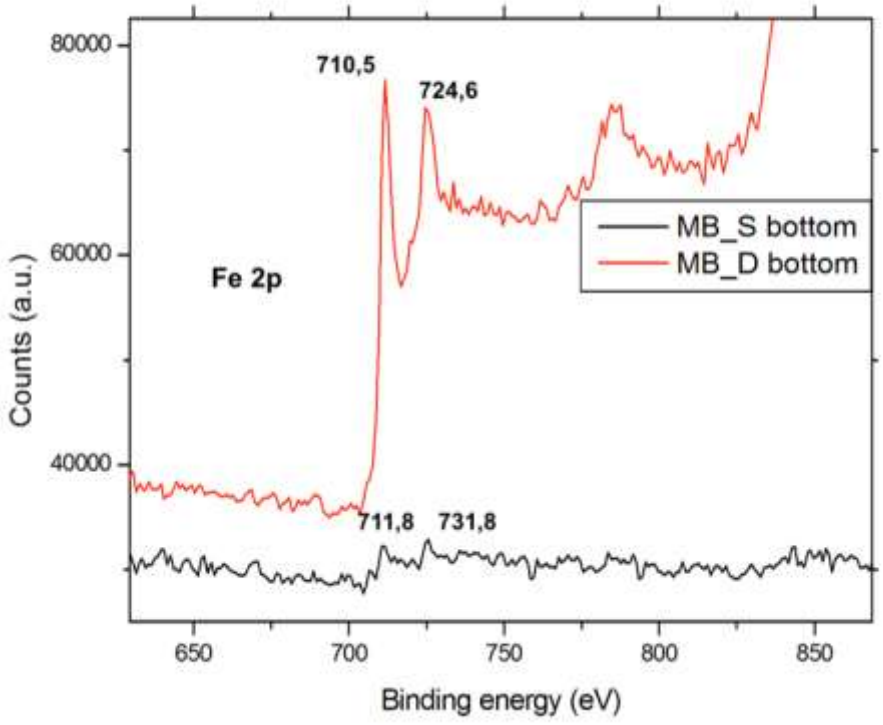

Figure 10. XPS spectra of MB_S and MB_D (dried at 23 °C and RH=60%) coating-steel surface after detaching from the steel.

3.2.4 Electrochemical characterization

Electrochemical impedance spectroscopy (EIS) was used to evaluate the corrosion protection of the synthetized latexes on the coated steel; the effect of phosphatization (mediated by interaction between polymer particles and steel surface), coating thickness and drying conditions were investigated. Table 3 summarizes the impedance modulus values (|Z| at 10^{-2} Hz, collected after 500 h of immersion in 3.5 wt% NaCl solution) obtained from Figure 11, where MB_D and MB_S, dried at different conditions, are plotted. MB_S2 and MB_S3 are films dried at the same drying conditions as the film in Figure 3b, but with different thickness, while MB_S1 is the film dried at low drying rate, as the film in Figure 3d. Bare steel (labeled Steel) was used as reference. It is worth to point out that values of impedance modulus of 10^9 Ω cm^2 or higher represent the maximum values achievable by the instrument.

Table 3. Properties and anticorrosion performances of MB series coatings

Latex	Specimen tag	Average thickness (μm)	Drying conditions		Ph*	Flash rust	IZI (Ω cm^2) **
			T (°C)	RH (%)			
MB_S	MB_S1	30	23	60	yes	no	10^9-10^{10}
	MB_S2	30	23	43	no	no	10^9-10^{10}
	MB_S3	90	23	43	no	no	10^9-10^{10}
MB_D	MB_D1	30	23	60	no	yes	10^9-10^{10}
None	Steel	-	-	-	-	-	10^3

* Phosphatization

** Values collected at 10^{-2} Hz after 500 hours of immersion in 3.5 wt% NaCl solution

All coatings show great corrosion protection due to the capacitive behavior, with impedance modulus values higher than 10^9 Ω cm^2 compared to that of bare steel at 10^3 Ω cm^2. Usually, the

medium-low frequency window (from 1 to 10^{-3} Hz) provides information of the coating/metal interface (e.g. charge transfer resistance and double layer capacitance related to the corrosion process, resistance of the formed oxides and capacitance related to passivation of the interface, etc.), while the high frequency range (from 10^{5} to 1 Hz) provides information of the barrier response of the coating [53, 54]. Considering the low frequency range, the impedance modulus was similar for all coatings and substantially higher than the reference substrate (more than 6 order of magnitude higher than bare steel). Neither the coating cast at lower relative humidity (without phosphatization layer MB_S2) nor the coating with higher thickness (MB_S3) present any noticeable difference in the whole frequency range of Bode plot; namely, at the mild conditions of exposure (500 h in a solution of 3 wt% of NaCl) the performance of the coatings was very similar. The coating made out of the conventional surfactant did also present the same performance. This is indicative of the good barrier performance of the copolymer system employed in all coatings under the mild exposure conditions, independently of the phosphate layer formation.

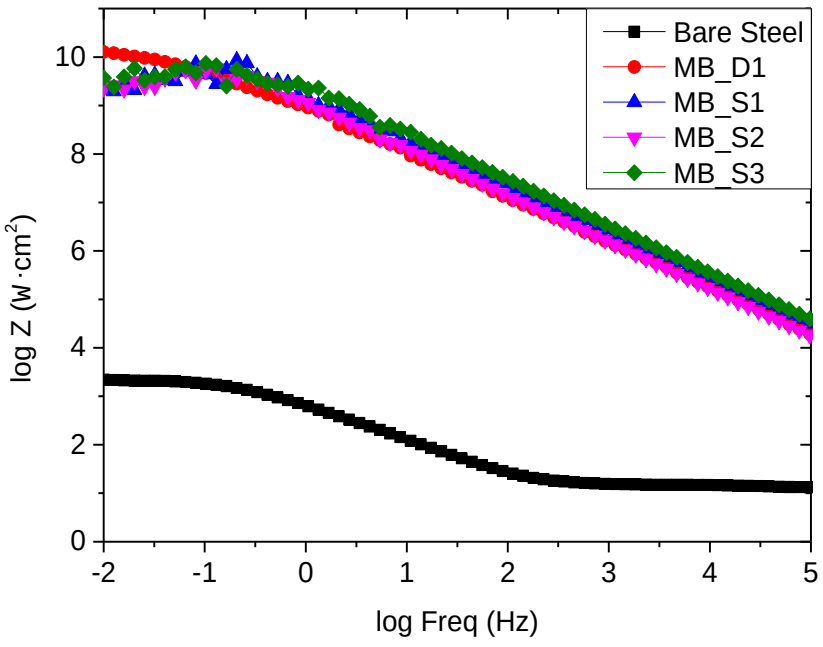

Figure 11. Bode plot showing the log |Z| vs. log Frequency of MB_D1, MB_S1, MB_S2 and MB_S3 after 500 h immersion in 3.5 wt% NaCl solution.

In order to assess the importance of the phosphatization layer, experiments using a harsh environment were carried out (e.g. accelerated salt spray tests). The results for steel specimens coated with these latexes are summarized in Table 4 and Figure 12.

Table 4. Salt spray test performances for MB_S and MB_D

Latex	Specimen tag	Film thickness (µm)	Drying conditions		IZI (Ω cm^2) *	
			T (°C)	RH (%)	144h	408h
MB_S	MB_S4	58	23	60	10^9-10^{10}	10^9-10^{10}
MB_D	MB_D2	60	23	60	10^9-10^{10}	10^8

* Impedance modulus values at 10^{-2} Hz after 144 and 408 hours in salt spray test

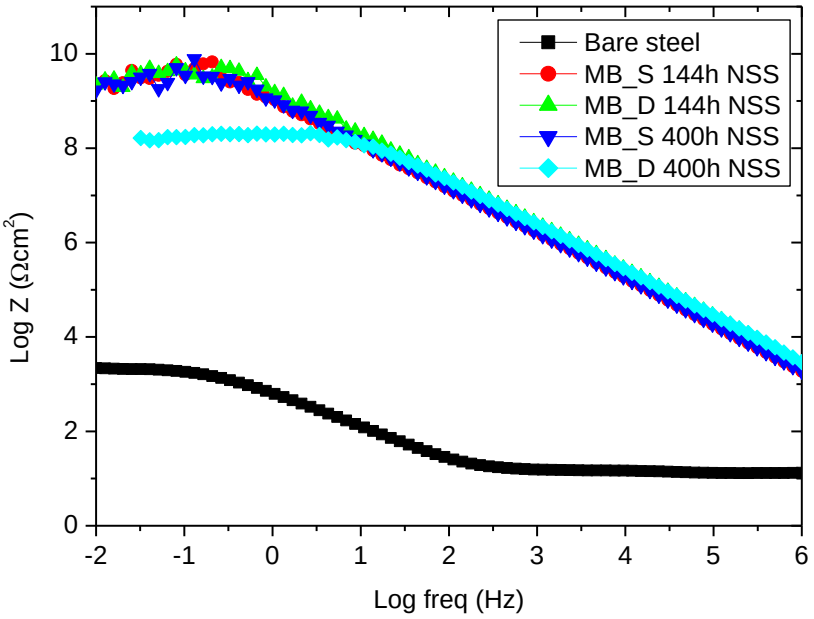

Figure 12. Bode plots of MB_S4 and MB_D2 after salt spray test at different exposure times.

Figure 11 shows the impedance diagram after different exposure periods in the NSS chamber. Although the barrier protection remained intact after 144 h of exposure for both coatings, the

influence of substrate phosphatization showed up after 400 h. In fact, the impedance modulus of MB_D2 (at low frequency range) dropped to $\approx 10^8$ Ω cm^2 while MB_S4 maintained the high value of a capacitive system (10^{10} Ω cm^2). It may indicate that the metal/coating interface is remaining intact, maintaining the passive state whilst the MB_D2 interface starts to fail.

NSS results confirm the enhanced corrosion protection of MB_S coating by a synergetic effect of good barrier properties together with the substrate phosphatization. In fact, the permeation of water and ions through MB_D2 started to be more effective (see Supporting Information) and, due to the absence of a passive layer at the coating/substrate interface, the corrosion mechanism occurred for this sample.

4. CONCLUSIONS

Poly(MMA-co-BA) latexes with phosphate functionalities (MB_S) were successfully synthetized by seeded semibatch emulsion polymerization by using a polymerizable phosphate surfactant (SIP).

When MB_S latex was applied on low carbon steel, it was found that the phosphate functionalities, bearing from SIP, were able to phosphatize the steel surface under slow drying rate (T=23 °C and RH= 60%). The formation of thin iron phosphate layer at the metal-coating interface was demonstrated by energy dispersed X-rays analysis (EDX), FTIR and XPS analysis.

Coatings made from these latexes yielded a phosphatization thin layer on steel substrates when dried at relative humidity higher than 60 % at room temperature. This layer plays a very important role on the anticorrosion properties of these coatings. It was found that in harsh exposure conditions the coatings that contained the in-situ produced phosphatization layer were able to present excellent corrosion after 400 h in salt-spray chamber, whereas latexes produced with the

same composition but using a conventional non-polymerizable and non-phosphate containing group failed and corrosion started on the steel substrates. This opens the possibility to use this functional waterborne dispersion in paint formulations that might require little or no anticorrosion pigments to be used.

SUPPORTING INFORMATION

Graphs showing the conversion and particle size evolution during MB_S and MB_D synthesis; TEM image showing the homogeneous morphology of the copolymer particles; Graph showing the drying kinetics of the film cast from MB_S and MB_D and the microscopy analysis of the cross sectioned film; Table summarizing the mechanical properties of the films cast from synthetized latexes; Graph showing the water uptake behavior of films cast from MB_S and MB_D. FTIR spectra of MB_S coating dried at high drying conditions, detached from the steel substrate; XPS patterns of MB_S and MB_D detached coatings.

ACKNOWLEDGMENT

The authors would like to thank the financial support received from the Basque Government (ETORTEK IE14-323, ELKARTEK KK-2017/00096, KK-2018/00108 and IT-373-10), and from the Spanish Government (MINECO CTQ -2017-87841-R). The authors would like also to thank for technical and human support provided by SGIker of UPV/EHU and European funding (ERDF and ESF).

REFERENCES

1. Hihara, L. H., Chapter 1 - Electrochemical Aspects of Corrosion-Control Coatings. In *Intelligent Coatings for Corrosion Control*, Tiwari, A.; Rawlins, J.; Hihara, L. H., Eds. Butterworth-Heinemann: Boston, 2015; pp 1-15.

2. Groysman, A., Corrosion Phenomena. In *Corrosion for Everybody*, Springer Netherlands: Dordrecht, 2010; pp 53-108.

3. International Measures of Prevention, Application and Economics of Corrosion Technology (IMPACT). *NACE international* **2013**.

4. Funke, W., Problems and progress in organic coatings science and technology. *Progress in Organic Coatings* **1997,** *31* (1), 5-9.

5. Ulaeto, S. B.; Rajan, R.; Pancrecious, J. K.; Rajan, T. P. D.; Pai, B. C., Developments in smart anticorrosive coatings with multifunctional characteristics. *Progress in Organic Coatings* **2017,** *111*, 294-314.

6. Kendig, M.; Mills, D. J., An historical perspective on the corrosion protection by paints. *Progress in Organic Coatings* **2016,** *102*, 53-59.

7. Montemor, M. F., Functional and smart coatings for corrosion protection: A review of recent advances. *Surface and Coatings Technology* **2014,** *258*, 17-37.

8. Arthur, D.; Jonathan, A.; Ameh, P.; Anya, C., A review on the assessment of polymeric materials used as corrosion inhibitor of metals and alloys. *International Journal of Industrial Chemistry* **2013,** *4* (1), 1-9.

9. Asua, J. M., Emulsion polymerization: From fundamental mechanisms to process developments. *Journal of Polymer Science, Part A: Polymer Chemistry* **2004,** *42* (5), 1025-1041.

10. Pilcher, G. In *Meeting the challenge of radical change: coatings R&D as we enter the 21st century*, Macromolecular Symposia, Wiley Online Library: **2002**; pp 1-16.

11. Pichot, C. , Delair, T. and Kawaguchi, H, Specialty Applications of Latex Polymers. In *Chemistry and Technology of Emulsion Polymerisation*, Ed. A. van Herk. **2013,** 283-305.

12. Kang, K.; Kan, C.; Du, Y.; Liu, D., Synthesis and properties of soap-free poly(methyl methacrylate-ethyl acrylate-methacrylic acid) latex particles prepared by seeded emulsion polymerization. *European Polymer Journal* **2005,** *41* (3), 439-445.

13. Rahman, O. u.; Kashif, M.; Ahmad, S., Nanoferrite dispersed waterborne epoxy-acrylate: Anticorrosive nanocomposite coatings. *Progress in Organic Coatings* **2015,** *80*, 77-86.

14. Haase, M. F.; Grigoriev, D. O.; Möhwald, H.; Shchukin, D. G., Development of Nanoparticle Stabilized Polymer Nanocontainers with High Content of the Encapsulated Active Agent and Their Application in Water-Borne Anticorrosive Coatings. **2012,** *24* (18), 2429-2435.

15. Nguyen, T.; Bentz, D.; Byrd, E., Method for measuring water diffusion in a coating applied to a substrate. *Journal of Coatings Technology* **1995,** *67* (844), 37-46.

16. Roulstone, B.; Wilkinson, M.; Hearn, J., Studies on polymer latex films: II. Effect of surfactants on the water vapour permeability of polymer latex films. *Polymer International* **1992,** *27* (1), 43-50.

17. Aguirreurreta, Z.; Dimmer, J. A.; Willerich, I.; de la Cal, J. C.; Leiza, J. R., Water Whitening Reduction in Waterborne Pressure‐Sensitive Adhesives Produced with Polymerizable Surfactants. *Macromolecular Materials and Engineering* **2015,** *300* (9), 925-936.

18. Aramendia, E.; Barandiaran, M. J.; Grade, J.; Blease, T.; Asua, J. M., Improving Water Sensitivity in Acrylic Films Using Surfmers. *Langmuir* **2005,** *21* (4), 1428-1435.

19. Liu, Y.; Soer, W.-J.; Scheerder, J. r.; Satgurunathan, G.; Keddie, J. L., Water vapor sorption and diffusion in secondary dispersion barrier coatings: A critical comparison with emulsion polymers. *ACS Applied Materials & Interfaces* **2015,** *7* (22), 12147-12157.

20. Jiang, B.; Tsavalas, J. G.; Sundberg, D. C., Water whitening of polymer films: Mechanistic studies and comparisons between water and solvent borne films. *Progress in Organic Coatings* **2017,** *105*, 56-66.

21. Aguirreurreta, Z.; de la Cal, J. C.; Leiza, J. R., Preparation of high solids content waterborne acrylic coatings using polymerizable surfactants to improve water sensitivity. *Progress in Organic Coatings* **2017,** *112*, 200-209.

22. Mistry, J. K., Ironing out stains. *European coating Journal* 2008.

23. Chimenti, S.; Vega, J. M.; Aguirre, M.; García-Lecina, E.; Díez, J. A.; Grande, H.-J.; Paulis, M.; Leiza, J. R., Effective incorporation of ZnO nanoparticles by miniemulsion polymerization in waterborne binders for steel corrosion protection. *Journal of Coatings Technology and Research* **2017,** *14* (4), 829-839.

24. US199209978, Lin C.-T. Additive package for in situ phosphatizing paint, paint and method **1994**.

25. Lin, C.-T., Green chemistry in situ phosphatizing coatings. *Progress in Organic Coatings* **2001,** *42* (3), 226-235.

26. Whitten, M. C.; Lin, C.-T., An in situ phosphatizing coating on 2024 T3 aluminum coupons. *Progress in Organic Coatings* **2000,** *38* (3–4), 151-162.

27. Yu, T.; Lin, C.-T., In-situ phosphatizing coatings III: A water-reducible alkyd baking enamel. *Journal of Coatings Technology* **1999,** *71* (895), 87-96.

28. US5191029A, Donno, D. Phosphorus-containing polymer compositions containing water-soluble polyvalent metal compounds. **1990**.

29. Reyes, Y.; Rodriguez, F. J.; del Rio, J. M.; Corea, M.; Vazquez, F., Characterisation of an anticorrosive phosphated surfactant and its use in water-borne coatings. *Progress in Organic Coatings* **2005,** *52* (4), 366-371.

30. Gonzalez, I.; Mestach, D.; Leiza, J. R.; Asua, J. M., Adhesion enhancement in waterborne acrylic latex binders synthesized with phosphate methacrylate monomers. *Progress in Organic Coatings* **2008,** *61* (1), 38-44.

31. Shi, X.; Nguyen, T. A.; Suo, Z.; Liu, Y.; Avci, R., Effect of nanoparticles on the anticorrosion and mechanical properties of epoxy coating. *Surface and Coatings Technology* **2009,** *204* (3), 237-245.

32. Andreeva, D. V.; Shchukin, D. G., Smart self-repairing protective coatings. *Materials Today* **2008,** *11* (10), 24-30.

33. Asua, J. M.; Schoonbrood, H. A. S., Reactive surfactants in heterophase polymerization. *Acta Polymerica* **1998,** *49* (12), 671-686.

34. Misawa, T.; Hashimoto, K.; Shimodaira, S., Formation of Fe(II)1·Fe(III)1 intermediate green complex on oxidation of ferrous ion in neutral and slightly alkaline sulphate solutions. *Journal of Inorganic and Nuclear Chemistry* **1973,** *35* (12), 4167-4174.

35. McGill, I. R.; McEnaney, B.; Smith, D. C., Crystal structure of green rust formed by corrosion of cast iron. *Nature* **1976,** *259*, 200.

36. Abdelmoula, M., Evidence for the Fe(II)-Fe(III) Green Rust "Fougerite" Mineral Occurrence in a Hydromorphic Soil and Its Transformation with Depth. *Hyperfine Interactions* **1998,** 112 (1-4), 235-238.

37. Kannan, A. G.; Choudhury, N. R.; Dutta, N. K., Electrochemical performance of sol–gel derived phospho-silicate-methacrylate hybrid coatings. *Journal of Electroanalytical Chemistry* **2010,** *641* (1), 28-34.

38. Keddie, J.; Routh, A. F., *Fundamentals of latex film formation: processes and properties*. Springer Science & Business Media: **2010**.

39. Lovell, P. A.; El-Aasser, M. S.; Lovell, P., *Emulsion polymerization and emulsion polymers*. Wiley New York: **1997.**

40. Buscall, R.; Corner, T.; Stageman, J. F., *Polymer Colloids*. Springer Netherlands: **1985**.

41. Provder, T.; Urban, M. W., *Film Formation in Coatings: Mechanisms, Properties, and Morphology*. American Chemical Society: **2001**.

42. Misawa, T.; Hashimoto, K.; Shimodaira, S., The mechanism of formation of iron oxide and oxyhydroxides in aqueous solutions at room temperature. *Corrosion Science* **1974,** *14* (2), 131-149.

43. Antunes, R. A.; Ichikawa, R. U.; Martinez, L. G.; Costa, I., Characterization of Corrosion Products on Carbon Steel Exposed to Natural Weathering and to Accelerated Corrosion Tests. *International Journal of Corrosion* **2014,** *2014*, 9.

44. T.S.N. Sankara Narayanan, Surface pretreatment by phosphate conversion coatings - a review. *Review on Advance Material Science,* **2005,** *9* (2), 130-177.

45. Tang, S.; Wang, W.; Chen, X.; Wang, J., Fluoridized iron phosphate as a novel adsorbent for selective separation/isolation of cytochrome c. *Journal of Analytical Bioanalytical Chemistry* **2011,** *401* (10), 3283-3292.

46. Ait Salah, A.; Jozwiak, P.; Zaghib, K.; Garbarczyk, J.; Gendron, F.; Mauger, A.; Julien, C. M., FTIR features of lithium-iron phosphates as electrode materials for rechargeable lithium

batteries. *Spectrochimica Acta Part A: Molecular and Biomolecular Spectroscopy* **2006,** *65* (5), 1007-1013.

47. Danmaliki, G. I.; Saleh, T. A., Effects of bimetallic Ce/Fe nanoparticles on the desulfurization of thiophenes using activated carbon. *Chemical Engineering Journal* **2017,** *307*, 914-927.

48. Salazar-Medina, A. J.; Gámez-Corrales, R.; Ramírez, J. Z.; González-Aguilar, G. A.; Velázquez-Contreras, E. F., Characterization of metal-bound water in bioactive Fe(III)-cyclophane complexes. *Journal of Molecular Structure* **2018,** *1154*, 225-231.

49. Hadži, D.; Sheppard, N., The Infra-Red Absorption Bands Associated with the COOH and COOD Groups in Dimeric Carboxylic Acids. I. The Region from 1500 to 500 cm⁻¹. *Proceedings of the Royal Society of London. Series A, Mathematical and Physical Sciences* **1953,** *216* (1125), 247-266.

50. Hwang, E. H.; Park, J. S.; Seong, H. G.; Kim, S. J., Analysis on surface film formed on high-strength carbon steels in acidic phosphate solution and its relationship with localized corrosion in a 3.5% NaCl solution. *Journal of Materials Research and Technology* **2019,** *8* (1), 1419-1426.

51. Wang, Y.; Sherwood, P. M. A., Iron (III) Phosphate (FePO4) by XPS. **2002,** *9* (1), 99-105.

52. Wang, Y.; Asunskis, D. J.; Sherwood, P. M., Iron (II) Phosphate (Fe3 (PO4) 2 by XPS. *Surface Science Spectra* **2002,** *9* (1), 91-98.

53. Pebere, N.; Picaud, T.; Duprat, M.; Dabosi, F., Evaluation of corrosion performance of coated steel by the impedance technique. *Corrosion Science* **1989,** *29* (9), 1073-1086.

54. Le Pen, C.; Lacabanne, C.; Pébère, N., Structure of waterborne coatings by electrochemical impedance spectroscopy and a thermostimulated current method: influence of fillers. *Progress in Organic Coatings* **2000,** *39* (2), 167-175.

SUPPORTING INFORMATION for

In-situ phosphatization and enhanced corrosion properties of films made of phosphate functionalized nanoparticles

*Stefano Chimenti [1], Jesús Manuel Vega [2], Eva García-Lecina [2], Hans-Jürgen Grande [2,3], María Paulis *[1], Jose Ramón Leiza *[1].*

1: POLYMAT, Kimika Aplikatua saila, Kimika Fakultatea, University of the Basque Country UPV/EHU, Joxe Mari Korta Zentroa, Tolosa Hiribidea 72, 20018 Donostia-San Sebastián, Spain.

2: CIDETEC, Parque Científico y Tecnológico de Gipuzkoa, Po. Miramón 196, 20014 Donostia-San Sebastian, Spain

3: POLYMAT, Polymer Science and Technology Department, Faculty of Chemistry, University of the Basque Country (UPV/EHU), 20018 Donostia-San Sebastian, Spain

Synthesis of phosphate functionalized latex

The instantaneous conversion of the latexes using Dowfax (MB_D) and Sipomer (MB_S) surfactants measured gravimetrically is plotted in Figure S1.

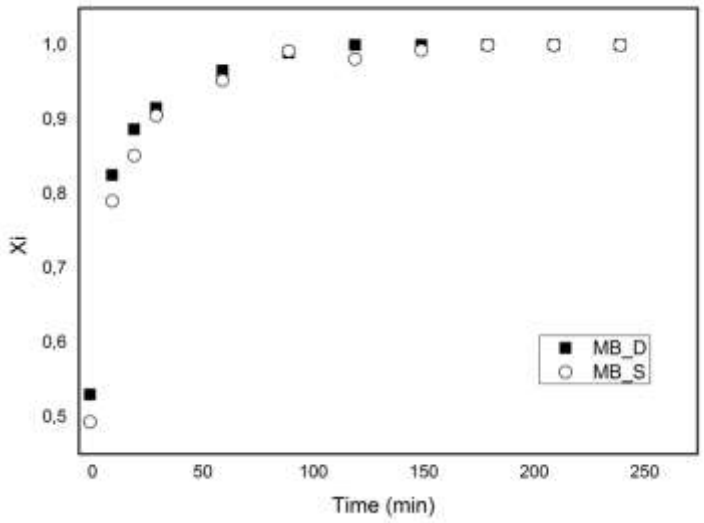

Figure S1. Evolution of the instantaneous conversion of MB_S and MB_D in the seeded semibatch emulsion polymerization.

Starved conditions (conversion higher than 90%) were obtained in the second stage of the process and the different surfactants, used in the second stage, hardly affected on the kinetic of the polymerization.

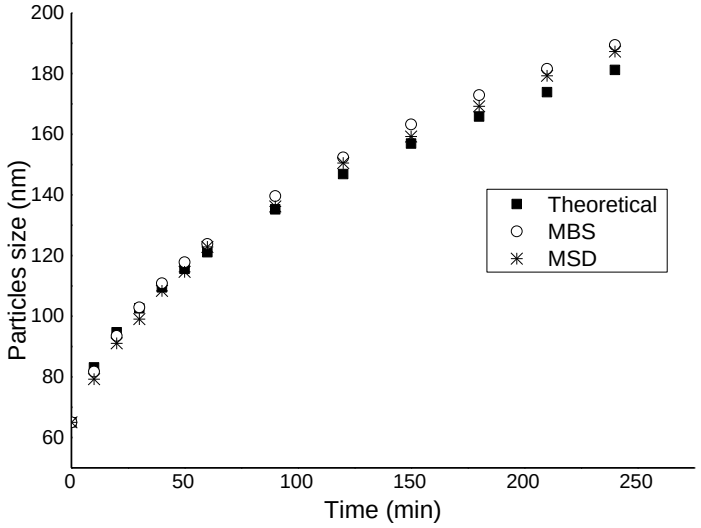

Figure S2. Time evolution of particle diameter for reactions MB_S and MB_D produced by the seeded semibatch emulsion polymerization.

The evolution of the particle size during the reaction for MB_D and MB_S (Figure S2) follows well the theoretical growth of the particles in absence of secondary nucleation or coagulation. The particle size slightly deviated from the theoretical evolution beyond 150 min, likely indicated some aggregation.

The morphology of the final polymer particles is homogeneous in shape and in electrical density as confirmed by TEM analysis in Figure S3. It can be seen that the average value of particles size (calculated on a sample of 20 particles) agreed with the values provided by dynamic light scattering of 189 nm.

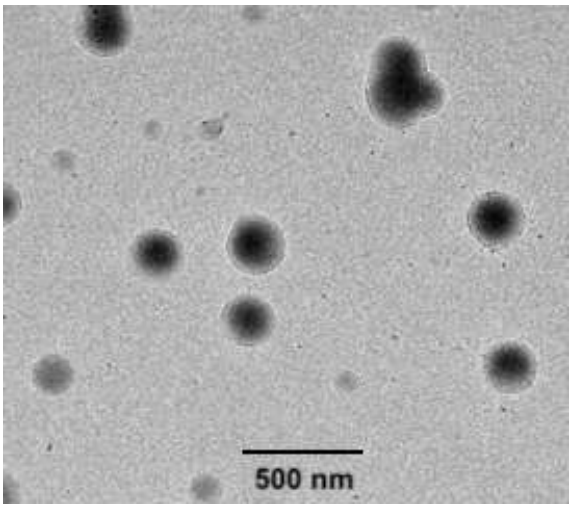

Figure S3. TEM micrograph of MB_S final latex.

Film formation process

Multispeckle Diffusing wave spectroscopy (MDWS) has been used to describe and to check the film formation process of the polymeric dispersions developed in this work. MDWS consist on sending a laser light into the film during its formation. Part of the incident coherent light is absorbed by the sample and the other part is backscattered and detected by a video camera through an interference image. During the film formation this interference image undergoes some changes which has been demonstrated to be related to the characteristic stages of the film formation process[1]; the speed of the change in the interference image is directly related to the motion of the scatterers (polymer particles) inside the sample.

Figure S4 shows the drying kinetics of MB_D and MB_S waterborne polymeric dispersions at 23ºC and 60% R.H. monitored by MDWS, which also highlights the characteristic stages of the film formation process and that are briefly described hereafter.

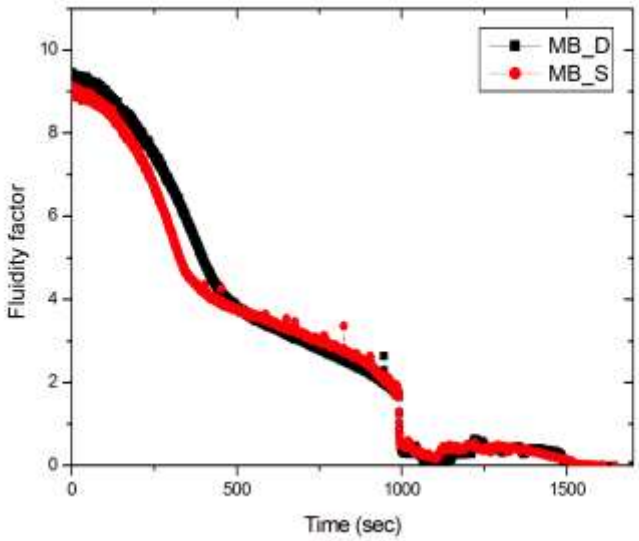

Figure S4. Drying kinetics of MB_D and MB_S latexes at 23ºC and 60% R.H., represented as variation of fluidity factor over the time, monitored by MDWS.

Initially the polymer particles are dispersed in the water phase and, as soon as the evaporation of the water proceeds, the particles get closer and the reduction of their mobility is showed in Figure S4 by a drop of the fluidity factor in the first 400 seconds. Then, the polymeric particles start to organize themselves as confirmed by a lower reduction of the fluidity factor (between 400 and 1000 seconds) which end up with the formation of a close packed array with water filled interstices (identified by a sharp drop after 1000 seconds). Within 1000 and 1500 second both samples experienced particles deformation, from spherical to hexagonal shape, as consequence of the interstitial water evaporation. After 1500 the fluidity factor results almost zero which indicates the disappearance of the particles boundaries and the occurrence of particles coalescence. The conclusion that can be withdrawn from Figure S5 is that the presence of the phosphated surfmer did not affect the drying process of the waterborne polymeric dispersion as the drying kinetics profiles almost overlapped.

SEM and TEM analysis of the cross sectioned film cast from MB_S (Figure S5 and S6 respectively) were also carried out to prove the coalescence of the particles. As can be seen, the film resulted coherent and no sign of lack of particle coalescence during the film formation (Figure S5) neither differences in the electron density (Figure S6) were detected.

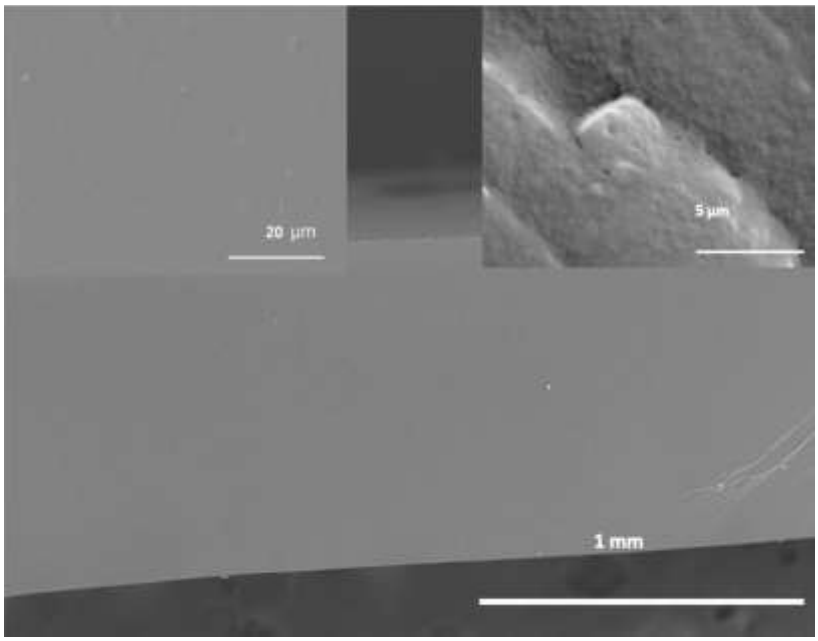

Figure S5. *SEM micrograph (cross-section) for film cast from MB_S.*

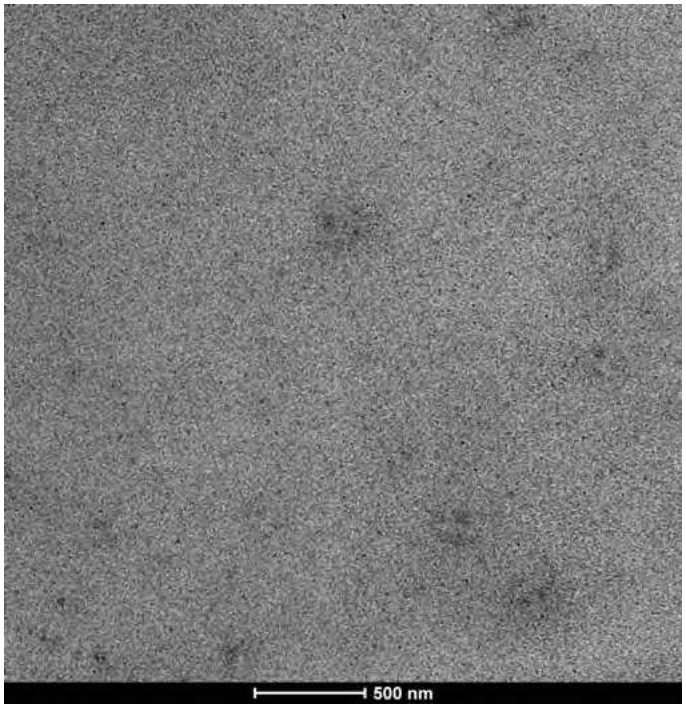

Figure S6. *TEM micrograph (cross-section) for film cast from MB_S.*

Water sensitivity and barrier properties were assessed by liquid water uptake (WU) test, that consists in monitoring for 15 days the weight gain by circular specimens (diameter = 24 mm, thickness= 2.3 mm) in water.

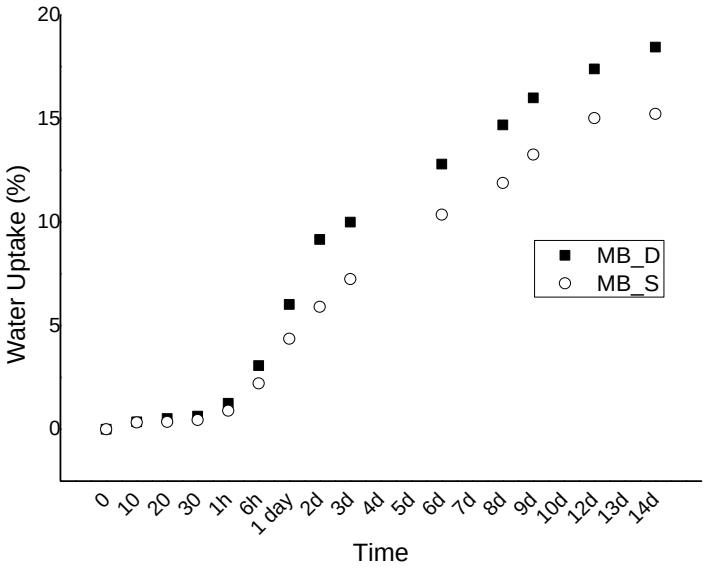

Figure S8. Water uptake evolution of MB_S and MB_D.

Coating properties and in-situ phosphatization

As it can be seen in Figure S8, when Sipomer was used, the water uptake of the final film results lower and hence the barrier properties higher if compared to the homologous with conventional anionic surfactant.

Figure S9 presents the FTIR spectra of the MB_S film detached from the steel surface after being dried at low relative humidity and Figure S10 a zoom of the low wavenumber region (high drying rate). As it can be seen, both surfaces, the one in contact with air and the one in contact with the steel present the same spectra, showing that no Fe phosphates were produced in this case.

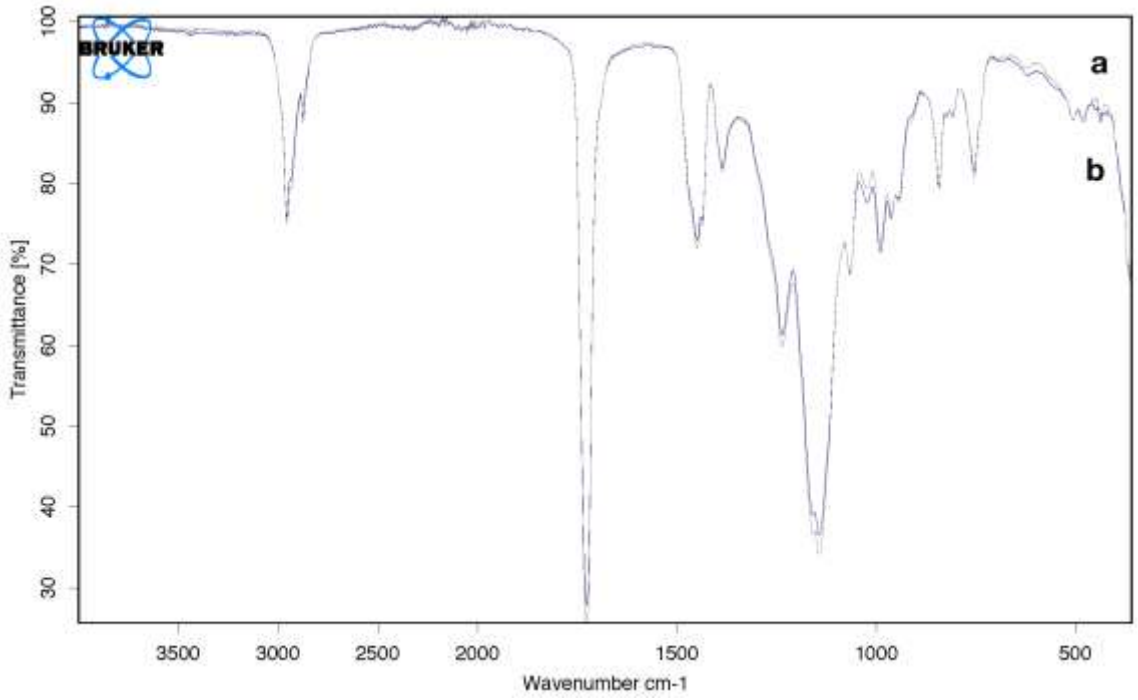

Figure S9. FTIR spectra of the MB-S film surface dried at low relative humidity at the coating-air (a) and coating-steel (b) interface.

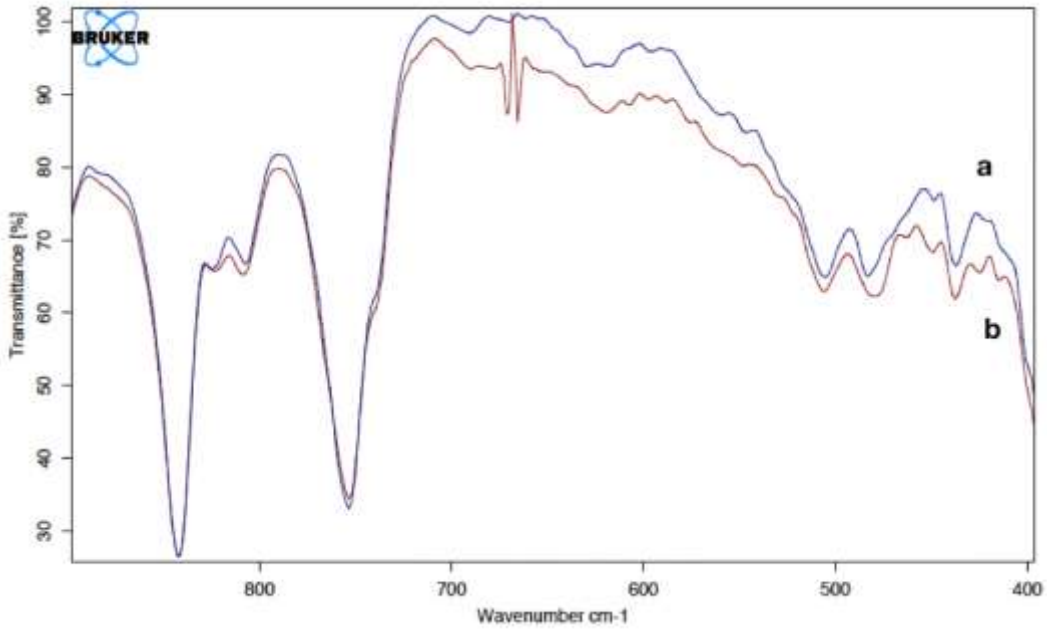

Figure S10 FTIR spectra of the MB-S film surface dried at low relative humidity at the coating-air (a) and coating-steel (b) interface.

Figures S11 and S12 present the XPS patterns of the MB_S and MB_D films detached from the steel surface after being cast at low relative humidity. As it can be seen, both surfaces at the coating-air interface resulted clean and the characteristic lines of C-H, C-C, O and C-O bonds are presents. On the other hands for the surfaces at the coating-steel interface, MB_D showed many lines related to the iron at different oxidation states characteristic of the Flash rust whereas, in the case of MB_S, as already mentioned in the main text, the presence of 2 tiny peaks of Fe 2P indicate the presence of a thin iron phosphate layer.

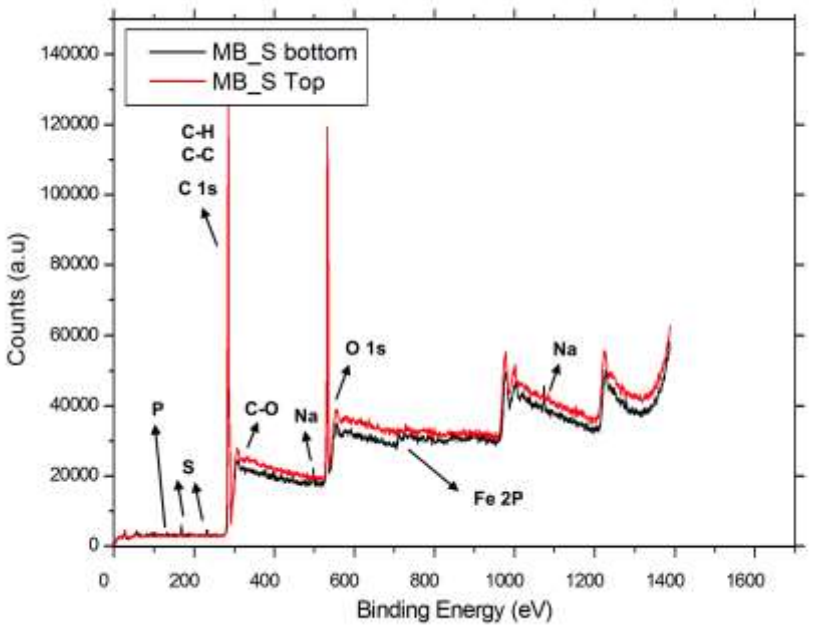

Figure S11 XPS patterns of MB-S film surface dried at 23 °C and RH= 60 % at the coating-air (MB_S Top) and coating-steel interface (MB_S Bottom).

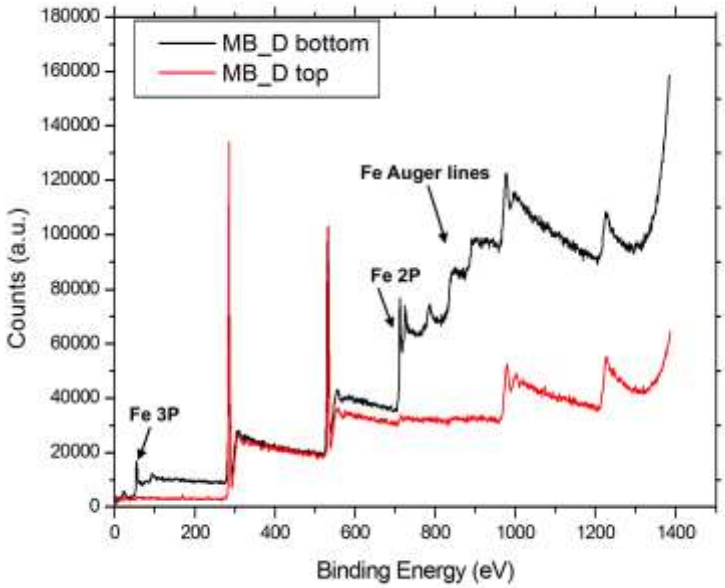

Figure S12 XPS patterns of MB-D film surface dried at 23 °C and RH= 60 % at the coating-air (MB_D Top) and coating-steel interface (MB_D Bottom).

The mechanical properties of the films cast from MB_S and MB_D latexes are reported in Table S1. As can be seen, the type of surfactant used did not affect the final properties of the resulting coatings.

Table S1 mechanical properties of the films cast at T= 23°C, RH=60%

Film	Elongation at break $*10^{-2}$ (%)	Ultimate Strength (MPa)	Young's Modulus $*10^{-2}$ (MPa)	Toughness $*10^{-6}$ (Jm^{-3})
MB_D	3.64 ± 0.59	8.53 ± 0.24	0.24 ± 0.13	33.72 ± 4.97
MB_S	3.62 ± 0.38	8.86 ± 0.70	0.21 ± 0.04	33.65 ± 5.16

1. Brun, A.; Dihang, H.; Brunel, L., Film formation of coatings studied by diffusing-wave spectroscopy. *Progress in Organic Coatings* **2008,** *61* (2), 181-191.